PERGAMON

International Journal of Solids and Structures 39 (2002) 449–465

INTERNATIONAL JOURNAL OF SOLIDS and STRUCTURES

www.elsevier.com/locate/ijsolstr

Structural cell of particulate elastomeric composites under extension and compression

V.V. Moshev *, L.L. Kozhevnikova [1]

Institute of Continuous Media Mechanics, Russian Academy of Science, Academic Korolev Street 1, 614013 Perm, Russia

Received 21 September 2000

Abstract

A unit cell of a specified shape under specified loading conditions has been investigated under extension and compression to get insight into microstructural mechanisms controlling macroscopic behavior of particulate polymeric composites. A variety of the boundary-value problems in the framework of large deformations have been solved. The comparative analysis has been carried out aimed at the clarifying the difference between the extended and compressed states of structural cells. The calculations have corroborated greater strength of cells under compression that agree well with common practice. It was established that, in the cells under compression, the separation of the matrix from the inclusion takes place instantly as with the loss of stability in contrast to quiet evolution in extension. It was found out that pore growth in cells under compression is four to five times lesser than under extension.

Keywords: Structural modelling; Particulate rubber composites

1. Introduction

Recently a specified structural unit cell for particulate elastomeric composites has been proposed and explored under tensile loading (Moshev and Kozhevnikova, 1997, 2000). The predictive capabilities of this cell have proved to be rather promising. So it seemed expedient to study in the like manner the behavior of the cell under compressive loading, since experience reveals that the response of particulate composites to compression differs considerably from that to extension. Elucidation of this difference on a microscale level seems to be of interest both from theoretical and practical points of view. This paper presents the results of such a comparative microstructural analysis with primary emphasis upon compression peculiar features. A transformation of the microstructural description into a continual one is offered and explored as a step bridging discrete and continuous representations the latter required by the design practice.

* Corresponding author. Address: Alexander Nevsky Street 28/16, 614113 Perm, Russia.
E-mail address: moshev@icmm.ru (V.V. Moshev).
[1] Address: Dedukin Street 6/105, 614013 Perm, Russia.

0020-7683/01/$ - see front matter
PII: S0020-7683(01)00204-9

Nomenclature

D	diameter of the structural cell
E_m	Young's modulus of the matrix
F	tension or compression force applied to the cell
G, B	parameters in the equation for the elastic potential of the matrix material
L	height of the structural cell
R	radius of the spherical inclusion
S	debonded surface on the inclusion
U	elastic potential of the neo-Hookean matrix material
W	displacement of the top end of the cell relative the bottom one
$\boldsymbol{C}$	Cauchi–Green deformation tensor
$\boldsymbol{g}$	unity tensor
$\boldsymbol{P}$	the second Piola–Kirchoff stress tensor
I_1, I_3	the first and the third invariants of the Cauchi–Green deformation tensor
T_a	adhesive bond fracture energy per unit of bonded surface of the inclusion
T_d	cohesive bond fracture energy per unit of bonded surface of the inclusion
U_m	elastic energy stored in the matrix volume of the cell
e_{ij}	component of the microstrain tensor within the matrix volume
e_1	maximum principal deformation in the matrix volume ($e_1 = \lambda_1 - 1$)
$(e_1)_b$	breaking strain of the elastomeric matrix
s_{ij}	component of the true microstress within the matrix volume
s_0	mean stress in the matrix $s_0 = (s_{11} + s_{22} + s_{33})/3$
λ_1	maximum microstretch within the matrix volume
$(s_0)_b$	dilation strength of the matrix
ε_z	deformation of the cell ($\varepsilon = W/L$)
ε_b	breaking strain of the cell
σ_{ij}	true stress component applied to the surface of the cell
φ	volume fraction of the inclusion in the cell, $\varphi = 16/3(R/D)^3$
σ_z	mean normal stress applied to the end of the cell

2. Theoretical background

2.1. Model cell geometry and boundary conditions

A general scheme of the accepted structural cell is shown in Fig. 1a. It represents an elastomeric cylinder (matrix) with a solid spherical inclusion (filler particle) at the center. The height, L, of the cylinder is equal to its diameter, D. A constant value, namely 2 cm, was assigned to the diameter of the cylinder and its height.

The cell is loaded uniaxially either by tension or by compression under zero external pressure. The geometry of the boundary conditions has been chosen so that, under deformation, the cell remained well compacted with other cells (Fig. 1b). Meeting this requirement makes ends of the cell to retain plane shape with the radial displacements not restrained and to keep the lateral surface as cylindrical one. This geometry conforms to the state of the cell located inside the close packing.

A remarkable feature characterizes the geometry adopted. Within the ensemble of the closely packed cells (Fig. 1b), the maximum filler volume is reached when the radii of the inclusions touch both the lateral

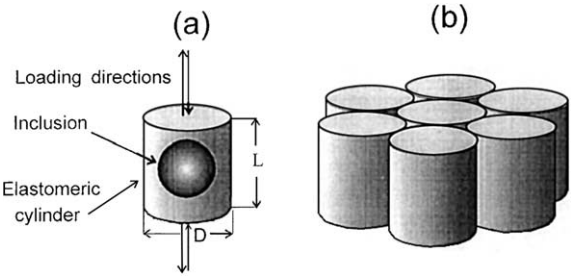

Fig. 1. Scheme of (a) the structural cell and (b) its assumed packing.

boundary and the ends of the cells. This volume is found to be equal to 0.607. This value chanced to be close to the ultimate volume filling, 0.605 (Chong et al., 1971; Farris, 1968) experimentally established in studies of suspensions filled with uniformly sized spherical particles. [2] This suggested that the behavior of a single structural cell might be thought to reflect rather adequately the property-concentration relations of realistic random system. This assumption was confirmed by Moshev and Kozhevnikova (1997, 2000). So this model has been accepted for studying its mechanical behavior under compression as well.

The tensile behavior of the cell broadly outlined depends on the initial state of the interface bond. If the sphere is supposed to be bonded to the matrix, a common mechanical evolution of the cell may be presented as it is shown in Fig. 2. During extension, this state is retained for some time (Fig. 2b). However, when the intensity of the stress–strain state within the matrix reaches some critical magnitude, the cell looses the capability to keep its continuity. For highly resilient matrices, it is the detachment of the matrix from the sphere that most often takes place as a primary damage event (Fig. 2c). An empty vacuole is formed above the pole zones of the sphere. It is supposed that matrix separation proceeds from the both poles of the inclusion in a similar manner. However, the cell might not be regarded as failed after the debond has occurred. It continues to resist extension although with a significantly reduced stiffness (Fig. 2d) until secondary damage comes about. This one is the break-down of the most strained matrix belt around the equator of the sphere (Fig. 2e). The secondary damage means the final failure of the cell. Though, another initial bond state originating matrix separation may be supposed, that, where the precursor debond patch is imposed at the pole of the inclusion. This case basically does not change the sequence of events shown in Fig. 2a–d.

Turning from the extension of the structural cell to its compression changes principally the pattern of its plausible mechanical evolution (Fig. 2f–h). Obviously, the polar zones, contrary to the former case, now must experience hydrostatic compression, while the equatorial region seems to be only slightly compressed. The damage mechanism is not so clearly seen as in the extension case. Hence subsequent analysis of this problem should be regarded as a largely speculative one. Nonetheless, some important points seem to be evident. First, in contrast to extension, maximum compressive displacement is definitely restricted by the height of the polar matrix width, determined by solid fraction volume. For moderate solid volume fraction of 30% it equals merely 0.23 of the radius of the cell, while tensile displacements accompanied by vacuole formation may be 10 times greater. Second, compressing polar matrix layer to zero width leads to a steep rise in compressive stresses tending to infinity. Hence, this part of the matrix volume seems to be most ready

[2] The value of 0.605 should not be identified with a well-known highest random packing density of 0.64 for uniform-sized spheres (Scott, 1962; Haughtey and Beveridge, 1969). The latter case represents a fixed rigid structure unable to continuous damageless deformation. In order to get deformable composition, the interparticle spaces should be somewhat increased, i.e., solid volume fraction should be somewhat decreased. The sought-for degree of the minimal rarefaction for the highest packing has been just one established experimentally by Chong et al. (1971).

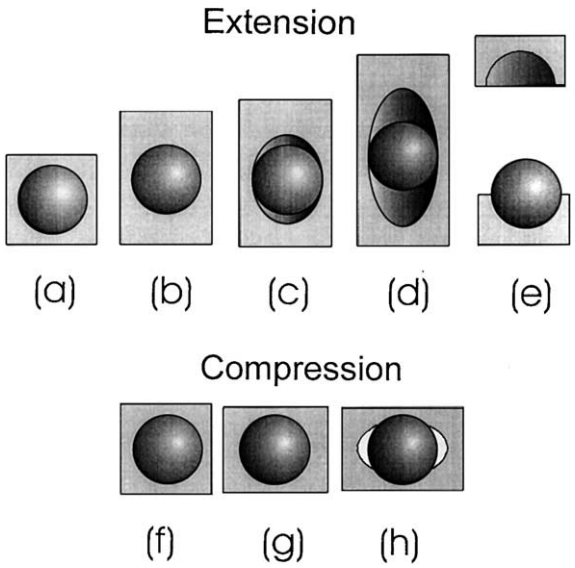

Fig. 2. Comparison of mechanical evolutions of the cell in tension ((a) initial; (b) extended before separation; (c) the same after separation; (d) extended separated; (e) ruptured) and in compression ((f) initial, (g) compressed before separation, (h) the same after separation).

for releasing accumulating elastic energy via some damage rearrangement. For instance, if a precursor debond patch occurs at polar region, then a release of elastic energy of the matrix might be thought of in form of the close debond spreading towards the equator as long as contact normal interfacial stresses remain negative. Matrix separation from the inclusion at the equatorial zone, as shown in Fig. 2h, might not be ruled out, as well. Some suggestions concerning conditions of the final failure of the cell under compression will be discussed later on.

No frictional resistance is taken into account in the cases, where the detached matrix is forced to slide along the inclusion surface.

2.2. Elastic properties of constituent materials

The approach adopted in this paper is purely elastic one. Only an equilibrium time-independent process is examined. The matrix phase is represented by a slightly compressible elastomer characterized by the elastic potential with two material parameters

$$U = G/2(I_1 - 3) + B/8(I_3 - 1)^2.$$

Here the first item of the sum represents neo-Hookean elastic potential for incompressible material, where I_1 and I_3 are the first and the third invariants of the Cauchy–Green deformation tensor, $\boldsymbol{C}$. G is a material constant, whose value is taken equal to 0.1 MPa, which corresponds to the shear modulus at small deformations. B is a second material constant that may be regarded as a bulk modulus at small deformations. Its value is taken to be 5 MPa which corresponds to Poisson's ratios about 0.49 that recently has been established by Blatz and Kakavas (1993), who experimented on realistic elastomers, inevitably containing small amounts of microscopic gas inclusions. The Young's modulus defined by the above basic parameters is equal to 0.298.

The type of the neo-Hookean elastic potential adopted above is based on the approach developed and reasoned soundly earlier by Rogovoy (1988) and Kozhevnikova et al. (1993) for a wide class of incompressible and nearly incompressible elastomers.

State equation derived from Eq. (1) has the form

$$\frac{1}{2}\boldsymbol{P} = \left(\boldsymbol{g} - I_3\boldsymbol{C}^{-1}\right)\frac{G}{2} + \frac{B}{4}(I_3 - 1)I_3\boldsymbol{C}^{-1},$$

where $\boldsymbol{P}$ is the second Piola–Kirchoff stress tensor, $\boldsymbol{g}$ is the unity tensor.

The solid sphere is taken to be perfectly rigid.

2.3. Damage criteria in structural cells

2.3.1. Extension case

Knowledge of the stress–strain state in the volume of the cell together with the characteristics of constituent materials, controlling damage appearance and evolution, is, clearly, the background for establishing the location and specificity of damage origination and evolution. It is assumed that the solid sphere is not only perfectly rigid but also non-destructive. So matrix volume and sphere–matrix interface remain the only vulnerable localities in the cell's volume.

Available experimental data allow us to get more comprehensive idea about basic mechanisms of the primary damage origination. Oberth and Bruenner (1965) observed that the separation of the matrix from the filler during extension was always preceded by formation and growth of many closely spaced tiny cavities within the matrix phase near the polar area of the inclusion, where the highest hydrostatic tension is created. The thin membranes separating these cavities bursted with creation a debond patch transforming thereupon into the open curvilinear crack propagating along the inclusion. When the matrix–sphere bond was considerable the crack run in the interior of the matrix phase with a thin matrix layer remaining intact on the surface of the sphere. Otherwise the crack divided the surface of the matrix from that of the sphere.

In actual composite materials precursor debonds patches of different sizes at different localities are available, as well, due to natural imperfection of industrial fabrication. When these debonds occur in critical points, they can also originate interfacial crack propagation.

Cho and Gent (1988) established that microcavitation in the matrix phase occurs, when its hydrostatic tension reaches some definite value. They stated that cavities stem from unstable elastic expansion of precursor tiny gas bubbles under the action of dilatant stress equal to 5/6 of the Young's modulus. Precursor gas babbles were shown to be naturally inherent to rubbers manufactured in industry (Blatz and Kakavas, 1993).

It follows from the above that critical hydrostatic tension $(s_0)_b$, for the matrix under consideration ($E_m = 0.298$) is bound to be

$$(s_0)_b = (5/6)0.298 = 0.248. \tag{1}$$

For the description of the crack propagation, Griffith's approach was used, which postulates that the debonded area will grow if the reduction in stored strain energy is equal to, or greater than, the energy, T, required for debonding (Gent, 1980; Kendall, 1971). Hence, the quantitative value of T is to be somehow determined.

It follows from the above, that there are two modes of the debond energy that should be specified. First, it is tearing energy of the matrix, T_d, that controls the crack propagation, when it occurs in the interior of the matrix phase. Second, it is the adhesive debond energy, T_a, specifying matrix–sphere interaction.

T_d value may be obtained from the paper by Gent and Tobias (1982), who investigated the correlation between tearing energy and Young's modulus of various rubbers. For hydrocarbon rubbers, this correlation may be approximated as

$$\log_{10} T_d = 5.0 - 0.50 \log_{10} E_m, \tag{2}$$

where T_d is the threshold energy in J/m^2 and E_m is the Young's modulus in Pa.

Remembering that in this study the Young's modulus of the matrix is taken to be 0.298 MPa, we have specified, by means of the above correlation, the threshold tear energy for the matrix equal to 150 J/m^2. Recall that this value is characteristic of the instance, when damage originates and progresses as a crack within the matrix phase adjacent to the surface of the inclusion.

When the adhesive debond energy occurs to be greater than the cohesive one then the crack growth evolution is controlled by the T_d value. Otherwise it is the adhesive debond energy, T_a, that leads this process of the crack separation. In other respects, both phenomena seem to be in perfect analogy.

After the crack separation has come to an end, the cell continues to resist extension with a reduced stiffness until the failure comes about. It is assumed that this occurs, when the local principle deformation, e_1, in the most strained matrix belt around the equator zone reaches its break-down value, $(e_1)_b$, inherent in the rubber under consideration (Fig. 2d).

2.3.2. Compression case

The cell's evolution under compression (Fig. 2f–h) reduces to squashing the matrix polar layers by the approaching cylindrical ends. It suggests that the negative hydrostatic stresses above the polar zone in the course of compression of the cell steeply grow tending to infinity. Hence the matrix cavitation and open crack formation in this conditions become impossible. On the other hand, just this locality seems to concentrate the most part of the elastic energy stored in the matrix phase. Under such conditions, precursor debond patches occurring at polar zones appear to be realistic sources of damage origination and evolution. If so, the precursor debond, regarded as a closed crack, begin spreading by matrix sliding along the surface of the inclusion with the plausible matrix separation only nearly the equatorial region, where positive normal stresses seem to be feasible.

It is assumed that, quantitatively, the growth of the original debond patch is controlled by the value of the adhesive T_a value, which is taken to be the same as that for the extension case, since this magnitude cannot be related to the mode of the energy formation in the interior of the matrix.

The mechanism of the final failure of the cell under compression looks more complicated than under extension. It is clear that, whether the interface debond takes place or not, the resistance of the cell to compression, in the framework of the problem under consideration, eventually tends to infinity. Obviously, the infinite resistance cannot be real phenomenon. It may be suggested that, in actual composite structures, considerable increase in compressive resistance should inevitably lead to the loss of the longitudinal stability of the cell, this event being beyond the scope of this study. Here the calculations of the compression curves will be stopped after beginning the steep increase in cell's resistance.

2.4. Matrix debonding evolution

Debond, arisen either from cavitation or from a precursor patch, starts spreading as a crack, either in open or in closed state, when the increment, dU_m, of the energy stored in the matrix during cell's loading reaches some definite magnitude, T, sufficient for creation a newly debonded interface area, dS.

This condition is usually expressed as follows:

$$dU_m/dS = T, \tag{3}$$

where T is the unit interface debond energy, determining the strength of the interfacial bond.

It is clear from the foregoing discussion that the magnitude T depends on the mode of the primary damage. If the crack propagates in the interior of the matrix, then T is identified with the proper tearing energy of the rubber matrix, T_d. If the crack originates from the precursor interface debond, T is identified

with the energy of the adhesive debonding, T_a. It should be remembered that T_d is a constant determined by the E_m value according to condition (2), while T_a is an independent magnitude ranging from zero to the magnitudes greater then T_d.

If T_a happens to be greater than T_d, then it is T_d magnitude that controls the process of the crack propagation. Otherwise, two modes of primary damage may be postulated. When the adhesive bond is perfect, the damage begins with the microcavitation ending in the primary interface debond patch formation growing under T_a control. When a random precursor patch near the polar zone is the source of the primary damage, then crack propagation proceeds under T_a value without preliminary microcavitation phenomenon. It follows from the above that in all instances T_d value determines the highest effort at which primary damage can occurs, other conditions being held unchanged.

Examine, as an example, the evolution of crack stemming from small precursor debond patch at the polar region. Let the adhesive debond energy T_a be a controlling parameter.

The current strain energy of the cell, U_m, is determined both by the cell deformation, $\varepsilon_z = W/L$, and the value of the current debonded area, S,

$$U_m = f_1(\varepsilon_z, S). \tag{4}$$

The condition (3) may now be rewritten as

$$T_a = \partial(f_1(\varepsilon_z, S))/\partial S = f_2(\varepsilon_z, S). \tag{5}$$

Taking T_a to be a constant magnitude during the entire process of the matrix debonding from $S = 0$ to $S = S_{max}$, opens an opportunity for establishing a definite correlation between ε_z and S.

The preliminary calculations for 30% solid volume fraction have shown that the area of the postulated precursor debond, giving rise to crack origination, should be taken about 0.05 of the total interfacial area for triggering crack propagation according to Griffith's approach. The response of the cell, having such initial debond patch is nearly the same as that of the perfectly bonded cell.

The response, F, of the cell in extension or compression is also a definite function of both the current values ε_z and S

$$F = f_3(\varepsilon_z, S). \tag{6}$$

Having obtained the relation between ε and S from Eq. (5), one can calculate tensile curve, F vs. ε_z, from Eq. (6) that is characteristic of the cell undergoing matrix–sphere debonding.

2.5. Calculation procedure

The detailed description of the calculation method is published elsewhere (Kozhevnikova et al., 1993). For the solution of the boundary value problem, a functional of a special form is offered and used

$$He(H, \overline{\boldsymbol{u}}) = \int_{V_0} \left(AH(I_3 - 1) - A^2(\alpha/2)H^2 + W_1(I_1) + (G/4)((I_3 - 1) - A\alpha H)^2 - \rho^0 \overline{\boldsymbol{K}}\,\overline{\boldsymbol{u}} \right) \mathrm{d}\boldsymbol{V}_0 - \int_{S_p^0} \overline{\boldsymbol{p}}\,\overline{\boldsymbol{u}}\,\mathrm{d}S_p^0, \tag{7}$$

where $A = BG/(2(B - G))$ and $\alpha = 4/B$; $\overline{\boldsymbol{u}}$ is the displacement vector; V_0 is the undeformed volume with volume forces, $\overline{\boldsymbol{K}}$, density, ρ^0, and the surface S_p^0, where forces, $\overline{\boldsymbol{p}}$, are applied; $AH = \sigma$ is the normalized quantity of σ.

The variations of this functional in H and $\overline{\boldsymbol{u}}$ lead to known variational equations of continuum mechanics for large deformations.

The finite element method was used for calculations. A typical sketch of the adopted finite element grid is shown in Fig. 3 for a solid volume fraction of 30%. Considering the geometry of the cell, a condensation of elements near the inclusion was performed.

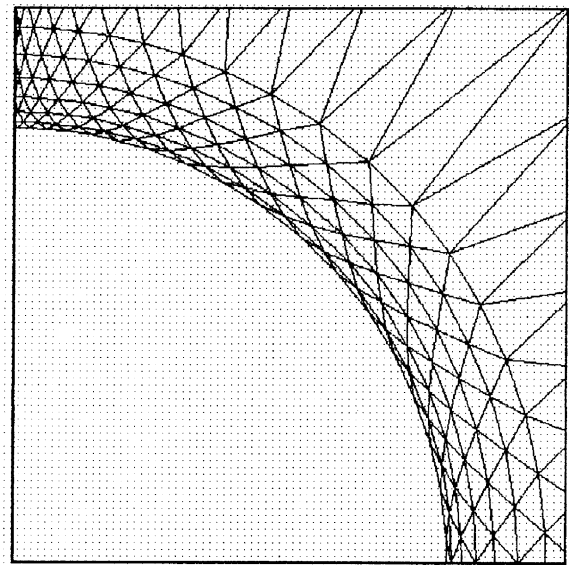

Fig. 3. Sketch of the finite element greed adopted for calculations for a filler volume fraction of 30%.

Displacement vector components and function H were approximated by the shape function Ψ_p and Φ_N. Then, the displacements become $u_p = \Psi_n u_p^n$ and the function $H = \Phi_N H^N$, where u_p^n is the value of the vector component up in n-node, while H^N is the H value in N-node.

A program was developed for the incremental load procedure, using triangular cylindrical finite elements with a square approximation to the displacement field, and linear functions H. In contact zones the condition for non-penetration was introduced.

Rogovoy (1988) proved the validity of the numerical results obtained with the calculation scheme adopted up earlier.

3. Microstress and microstrain distributions in the matrix phase of cells under extension and compression

3.1. Representation of the microscopic stress–strain state

In the framework of this paper, the distribution of stresses and strains within the matrix is defined solely by cell's axial deformation, ε_z. The external pressure is taken to be zero. It seems reasonable to examine separately the bonded, partly debonded and completely debonded states of the cell.

According to previous discussion, two representative quantities of the stress–strain state of the rubbery matrix are chosen for further analysis: the maximum principle strain, e_1, as an invariant characterizing the *intensity of deformation* and the mean stress, s_0, as a measure of *hydrostatic intensity of stress state*. In this paper the value of e_1 is presented as $e_1 = \lambda_1 - 1$, where λ_1 is the maximum principal stretch. The value of s_0 is the mean of three principal true stresses.

The quantitative data presented in the subsequent analysis should be regarded as illustrations of the phenomenon under discussion. They have been obtained from calculations for a cell containing 30% by volume solid phase, extended or compressed to 10%. The filler concentration chosen, dividing the low and high filler volume domains, seems to be the most appropriate for general examination.

Figures will present e_1 and s_0 distributions for imposed conditions as shadow patterns: the higher the level of the strain or stress the lighter the shadow. Such patterns are to be regarded primarily as qualitative estimations for getting general orientation, although most important numerical data needed for analysis are indicated in the appropriate localities.

3.2. Bonded cell

Fig. 4 presents e_1 and s_0 distributions under extension and compression. Strain patterns for extension are rather close to each other. The most strained localities are situated above the poles of the sphere and along its surface at an angle of about 45° with respect to the z-axis direction. For the adopted 30% volume filling, the maximum strains in the matrix are about 0.5 that is four to five times greater than the proper strain of the cell.

However, patterns of hydrostatic stress distributions depict considerable difference. High tensile hydrostatic stresses of about +0.2 MPa at polar zones, characteristic of extension, give place to still higher (absolute) mean compressive stresses of about −0.32 MPa under compression. At equatorial zones, hydrostatic compressive stresses of about −0.1 MPa under extension transform into moderate hydrostatic tensile stresses of about +0.05 MPa under compression.

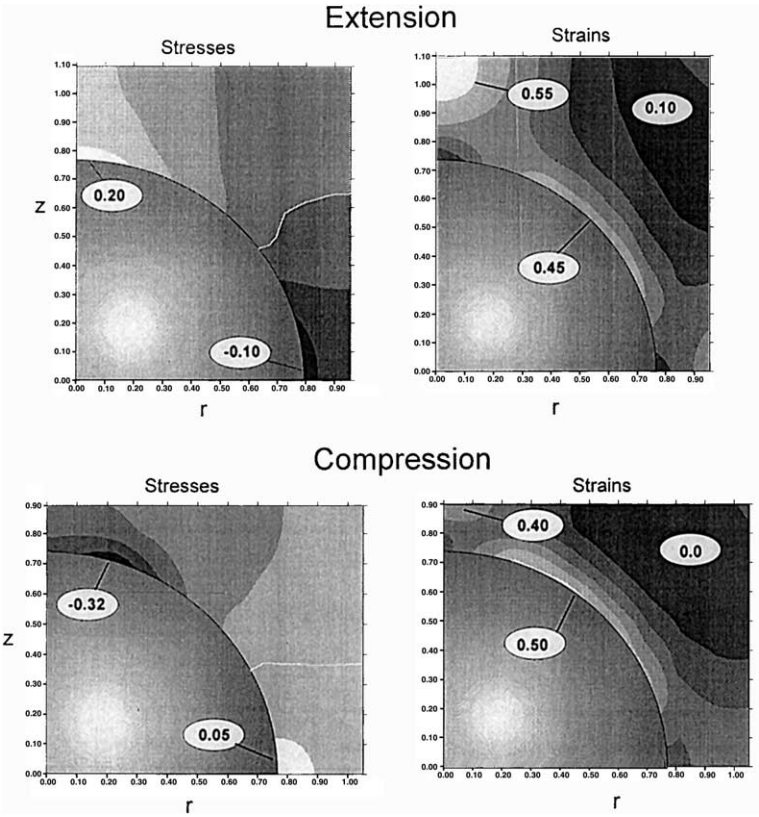

Fig. 4. e_1 and s_0 distributions in extension and compression for the bonded cell's state. White lines demarcate the regions of positive and negative mean stresses.

Fig. 4 gives a clear general idea about plausible sources and sites of the primary damage appearance. Under extension, these are the pole, creating crack origination, and interface localities at an angle of 45°, promoting crack propagation and vacuole opening. Under compression, it is the interface, where the matrix debond origination seems to be the most probable. In contrast to extension, this process may be realized solely as the matrix–sphere tangential disconnection followed by sliding of the torn matrix along the surface of the inclusion.

3.3. Partly debonded cell

A general estimation of the strain and stress distributions in partly debonded cells under extension and compression can be perceived from Fig. 5. The input condition for calculation ($T_a = 100$ J/m^2) has been adjusted so that the crack opening would be well outlined at the imposed 10% straining.

Under extension, the matrix detached from the polar zone forms a vacuole cavity drastically rearranging, stress distributions as compared with the extension case of Fig. 4. A withdrawn vault-like part of the matrix, that before exhibited the highest strains and tensile hydrostatic stresses, now experiences insignificant compression and is weakly strained, whereas the highest strains and stresses are moved to the stress concentration point—the tip of the crack.

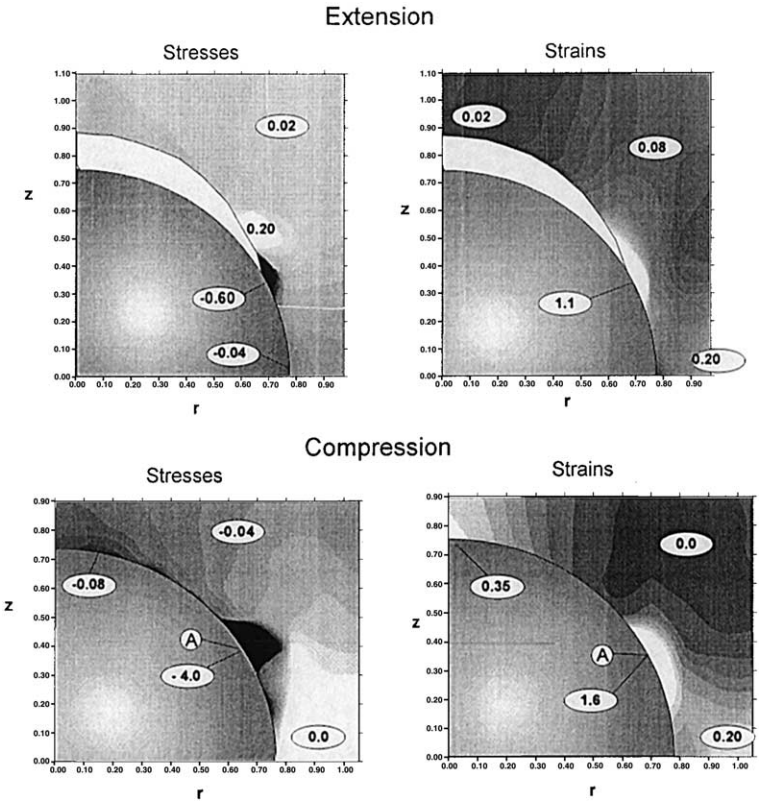

Fig. 5. e_1 and s_0 distributions in extension and compression for partly debonded cell. Zone of the matrix interface sliding is labeled by the white line with the end at point A.

Clearly, the finite element approach can provide only approximate estimations in this locality. Nevertheless, it gives some insight into the order of magnitude of the strains computed for the grid adopted. Calculated coefficients of the strain concentration are of the order of several tens.

Debonding under compression, postulated to originate from the precursor debond patch, also entails considerable change in the stress and strain distributions as compared with the compression case of Fig. 4: compressive mean stresses and strains are reduced considerably due to possibility of matrix sliding along the debonded interface. However a sharp outburst of stresses and strains appears in the point A dividing debonded area (white line) from the bonded one.

The e_1 and s_0 "compressive" distributions in Fig. 5 differ greatly from the corresponding "extensive" ones. A large volume of minor tensile hydrostatic stresses around vacuole under extension transforms into a poreless volume under hydrostatic compression. Low strains, characteristic of extension case, are contrasted with high strains for a compression one. The stress and strain concentration in the point of singularity under compression seems to be more intensive than under extension.

3.4. Debonded cell

After the debond propagation, during extension or compression, have reached the equator of the inclusion, the cell may be judged as fully debonded. Typical strain and stress distributions in completely debonded cells are exemplified in Fig. 6. Cavitations occur both under extension and compression. In the first instant, cavity is shaped as a vacuole, in the second as an empty belt around equator. Singular points

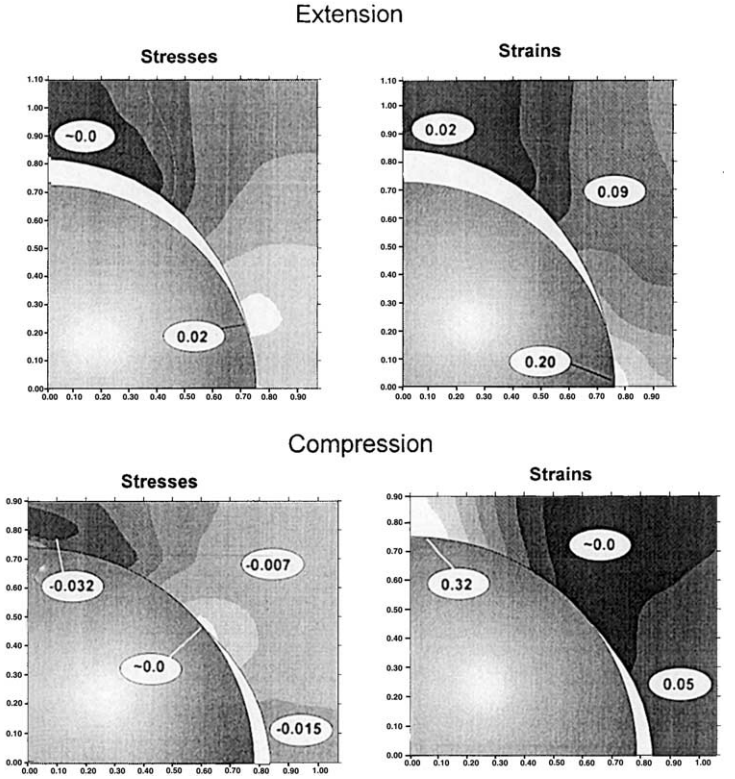

Fig. 6. e_1 and s_0 distributions in extension and compression for the debonded cell's state. No positive s_0 exists in compression.

disappear and with them the stress and strain concentrations. This is in a good agreement with the results of Dekkers and Heikens (1985) for a rigid sphere embedded into an infinite polymeric matrix. In extension, the strain magnification factor at the equatorial matrix belt now turns out to be about two and in compression at polar zone about three.

The general pattern of the stress and strain distributions of Fig. 6, as compared with the case of the partial debond (Fig. 5), remains essentially the same. Under extension, the hydrostatic stresses are positive in bulk with insignificant compression in the dome above the vacuole cavity. Under compression, the entire matrix volume experiences hydrostatic compression with a considerable increase at the polar zone.

4. Effective characteristics of cells

The foregoing analysis has been focused on the internal stress and strain states in structural cells under extension and compression. A transformation of *structural notions and relations*, used in solutions of boundary-value problems, into corresponding *macroscopic characteristics* of cells, now regarded as continuum formations, is of great theoretical and practical importance.

For this, a substitution of the microstresses, s_{ij}, and microstrains, e_{ij}, that have been used, say, for *inside-cell* analysis, for macroscopic stresses, σ_{ij}, and strains, ε_{ij}, of a larger scale level, i.e., that of the cell characteristic size, is needed. This allows the cell to be presented as some uniform material unit.

Based upon the assumed boundary conditions for cells, the normal nonuniform microstresses s_z and s_r at the ends and lateral area of the cell may now be substituted for their averaged values σ_z and σ_r that may be regarded as common sense stresses on the boundary of a continualized material unit. In the following analysis σ_z and σ_r will be presented as values related to the current cross-section of the cell model. In calculations, the relation between imposed axial displacement and searched-for radial displacement is adjusted so that the averaged σ_r value reduces to zero. The tensile strain of the cell, ε_z, is calculated simply as the ratio between displacement of the ends, W, and the initial height of the cell, L. Hence, the notion of the effective Young's modulus of the cell may be easily formulated as a ratio between σ_z and ε_z at adopted zero external pressure.

The macroscopic behavior of the cell model will be represented by its stress–strain and volume–strain curves. A particular form of these relations is a function of a number of the input parameters that are adopted as follows: $\varphi = 0.3$, $G = 0.1$ MPa, $B = 5.0$ MPa, $(e_1)_b = 2.0$. It is assumed that the interface separation (under extension or compression) originates from a small precursor debond patch, located at polar zone, with a crack propagating by the adhesive debond mechanism with $T_a = 100$ J/m^2.

4.1. Tensile and compression curves of the cell model

Tensile curve, $\sigma_z \sim \varepsilon_z$, of a cell calculated according the scheme adopted above is depicted in Fig. 7. The initial response of the cell both to extension and compression is characterized by the same initial modulus corresponding to the state of perfect bond. It is seen that detachment under extension starts at $\sigma_z = 0.10$ MPa ($\varepsilon_z = 0.11$), whereas that under compression at $\sigma_z = -0.17$ MPa ($\varepsilon_z = -0.18$). This calculation demonstrates a well-known experimental fact that strength of particulate composites under compression is usually essentially higher than that under extension.

Under extension, after the onset of the detachment has happened, a steep drop the stiffness of the cell takes place. However, the initial crack evolution diminishes the energy stored in the matrix to such a degree that additive energy input is needed for continuation of the crack propagation. This input is provided by the ever-continuing cell's extension. The greater becomes the separated zone, the lower becomes the rigidity of the cell, and the slower gaining energy needed for crack propagation until complete debond is achieved. Then the stiffness of the cell becomes stabilized, but at lower level as compared with the initial one.

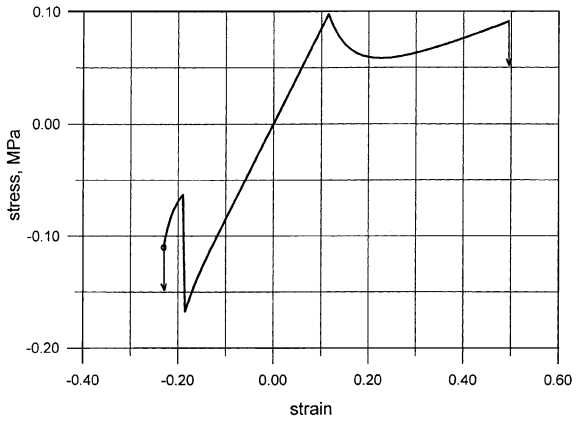

Fig. 7. $\sigma_z \sim \varepsilon_z$ relations for extension and compression at 30% filler fraction volume.

Under extension, the cell breaks down, when the maximum principle strain of the matrix at the equator reaches the breaking value equal to 2.0, as adopted above.

Contrary to extension, the energy accumulated in compression before start of the crack propagation has proved to be quite sufficient for complete debonding the matrix from the sphere without the need in the accessory outer energy input. So this transition might be regarded as an instant event.

With ever-continuing compression, a new increase in resistance starts but with the stiffness characteristic of the fully debonded state. Nevertheless, the boundary conditions inevitably lead to the unbounded increasing the resistance of the cell. The failure of the cell under strong compressive loading most likely takes the form of the loss of elastic stability with the violation the boundary conditions in the adopted modelling. The establishment of the strain at which the loss of stability comes about is beyond the scope of this paper. In our case, calculations have been stopped, when steep increase in the resistance of the cell came about.

Considerable distinctions between extension and compression curves for cells containing various solid volume fractions are clearly seen in Fig. 8 (for bonded systems) and Fig. 9 (for debonded from the outset ones). The stiffness of the bonded cells increases with filler volume fraction both in extension and compression. This is not so in the case of debonded cells, where the stiffness diminishes with filler volume fraction under extension, but keeps increasing under compression.

4.2. Volume changes in extension and compression

Difference in the location and shape of pores appearing under extension and compression is depicted in Fig. 6. An example of volume changes accompanying extension and compression of the cell with the 30% filler volume is shown in Fig. 10. While the cell remains in the bonded state the volume changes with a good approximation may be neglected both for extension and compression. After the separation has occurred under extension, pore volume grows monotonously tending to linearity. Nothing impedes volume growth until failure occurs. In our example, volume increase reaches 0.16 by the time of failure of the cell. Under compression, volume increase, in contrast, takes the form of a stepwise jump transferring at once the system from the complete bond to the complete debond with the following quiet volume increase on further compression though with a lesser volume increment.

Maximum volume changes exhibit completely debonded cells. Fig. 11 demonstrates volume changes of such cells under extension and compression at various filler volume fractions. Here again considerable

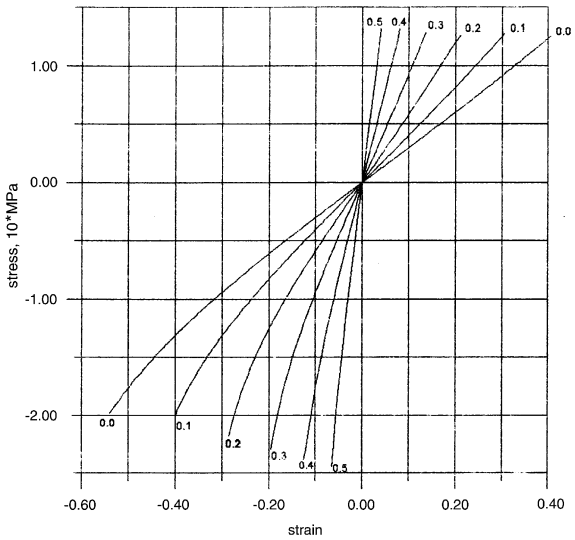

Fig. 8. Tensile and compression curves for bonded cells at various filler volume fractions indicated near the curves.

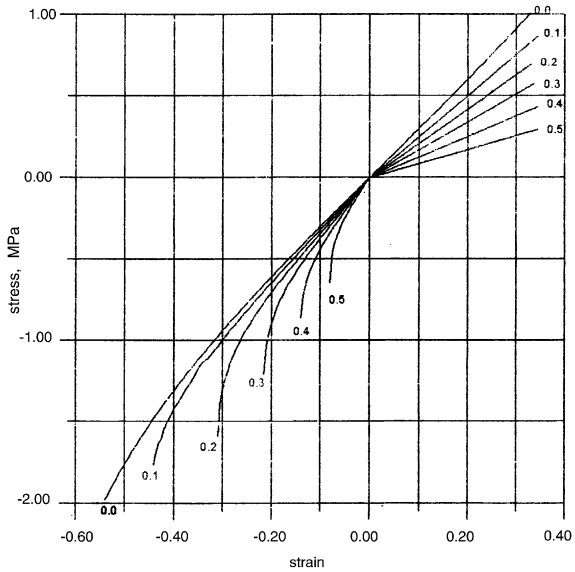

Fig. 9. Tensile and compression curves for debonded cells at various filler volume fractions indicated near the curves.

distinction between the response of the cells to the mode of loading is observed. At the same strains, volume changes under extension are considerably higher than those under compression. The growth of vacuoles in the former case is not restrained and increases with filler volume fraction. In contrast, compression impedes pore formation due to the specific boundary conditions (buckling excluded) and restriction in the axial displacement. Moreover, when the filler volume fraction becomes more than 0.4, ultimate pore volume starts to diminish tending to zero at the radius of inclusion equal to the radius of the cell's cylinder.

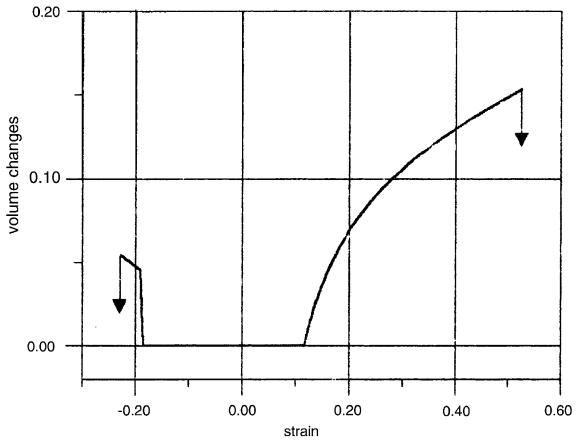

Fig. 10. Volume change in extension and compression at 30% filler fraction volume.

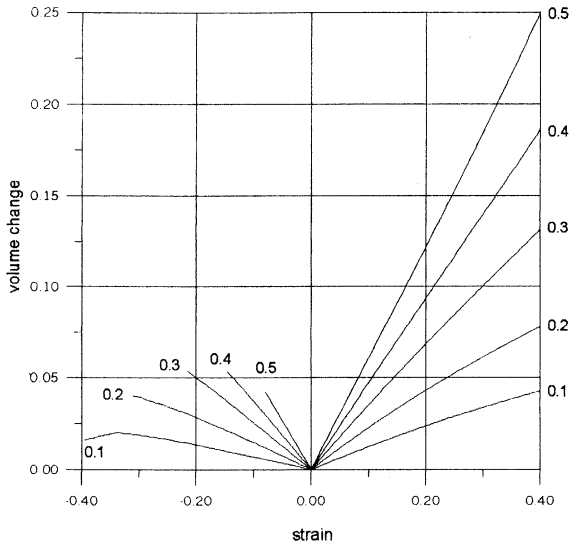

Fig. 11. Volume changes of the debonded cells in extension and compression at various filler volume fractions indicated near the curves.

5. Discussion and conclusions

A unit cell of a specified shape under specified loading conditions has been investigated under extension and compression to get insight into microstructural mechanisms controlling macroscopic behavior of particulate polymeric composites. A variety of the boundary-value problems in the framework of large deformations have been solved. The comparative analysis has been carried out aimed at the clarifying of the difference between the extended and compressed states of structural cells.

Natural submicroscopic imperfections of the unit structural cells are considered as the root sources of the primary microdamage origination. These are tiny gas inclusions inherent in elastomers and virgin

debond patches of various sizes and localities at the rubber–sphere interface. The role of the latter ones, localized at the most vulnerable polar zone of the structural cell, is demonstrated.

The establishment and analysis of the microstress and microstrain patterns within the matrix phase and along the interface of the cell in bonded, partly bonded and debonded states help to understand some of macroscopic peculiarities incident to extension and compression of composites.

It is known from experience that the strength of particulate composites under compression is commonly higher than that under extension. In modeling, the same result has been obtained (points A and B in Fig. 7). The calculations have shown that, under compression, an essentially higher strain energy is required for strating crack propagation of the precursor debonds according to Griffith's postulate. This automatically leads to higher critical stresses in comparison with the extension case.

In contrast to the smooth prolonged separation process during extension of the cell, the detachment of the matrix under compression occurs instantaneously. It may be safely suggested that this distinction is due to the accumulation of the higher stored elastic energy in the matrix phase, prior to the debond onset, sufficient for complete detachment of the matrix from the sphere, at least for the particular case under consideration.

While failure of the cell in extension depends on the breaking strain of the matrix phase that, in its own, varies over a wide range from about 100% to 1000%, compressive strains are strictly determined by the polar layer widths in the structural cell, which, for instance, for 30% solid volume fracture is nothing more than 0.234. Clearly, failure under compression must somehow precede reaching this limiting value. The most likely mechanism of the failure in this case is the loss of the longitudinal elastic stability, a phenomenon going beyond the scope of this work.

Quantitative data on pore forming in the cells under compression are obtained. It was found out that pore growth in cells under compression is four to five times lesser than under extension that is in qualitative agreement with the experience.

Acknowledgements

The financial support of the Russian Foundation of Fundamental Research and The Department of Science and Education of Perm region administration under Grant Number 01-01-96492 is greatly acknowledged.

References

Blatz, P.J., Kakavas, P., 1993. A geometric determination of void production in an elastic pancake. J. Appl. Polym. Sci. 49, 2197–2205.

Cho, K., Gent, A.N., 1988. Cavitation in model elastomeric composites. J. Mater. Sci. 23, 141–144.

Chong, J.S., Christiansen, E.B., Baer, A.D., 1971. Rheology of concentrated suspensions. J. Appl. Polym. Sci. 15, 2007–2021.

Dekkers, M.E., Heikens, D., 1985. Stress analysis near the tip of a curvilinear interfacial crack between a rigid spherical inclusion and a polymer matrix. J. Mater. Sci. 20, 3865–3872.

Farris, R.J., 1968. Prediction of the viscosity of multimodal suspensions from unimodal viscosity data. Trans. Soc. Rheol. 12, 281–301.

Gent, A.N., 1980. Detachment of an elastic matrix from a rigid spherical inclusion. J. Mater. Sci. 15, 2884–2888.

Gent, A.N., Tobias, R.H., 1982. Threshold tear strength of elastomers. J. Polym. Sci.: Polym. Phys. Ed. 20, 2051–2058.

Haughtey, D.P., Beveridge, G.S.G., 1969. Structural properties of packed beds—a review. Canad. J. Chem. Engng. 47 (4), 130–140.

Kendall, K., 1971. The adhesion and surface energy of elastic solids. J. Phys. D: Appl. Phys. 4, 1186–1195.

Kozhevnikova, L.L., Moshev, V.V., Rogovoy, A.A., 1993. A continuum model for finite void growth around spherical inclusion. Int. J. Solids Struct. 30, 237–248.

Moshev, V.V., Kozhevnikova, L.L., 1997. Highly predictive structural cell for particulate polymeric composites. J. Adhesion 62, 169–186.

Moshev, V.V., Kozhevnikova, L.L., 2000. Predictive potentialities of a cylindrical structural cell for particulate elastomeric composites. Int. J. Sol. Struct. 37, 1079–1097.

Oberth, A.E., Bruenner, R.S., 1965. Tear phenomena around solid inclusions in castable elastomers. Trans. Soc. Rheol. 9, 165–185.

Rogovoy, A.A., 1988. State equation and functional for weakly compressible and incompressible materials under large deformations. In: Mechanics of elastomers. Trans Krasnodar Polytech Inst., pp. 72–88, (in Russian).

Scott, G.D., 1962. Radial distribution of the random close packing of equal spheres. Nature 194 (4832), 956–957.